OFFICE OF NAVAL RESEARCH

Research Contract: N00014-90-J-1178
R&T Code: 413r008---01

Principal Investigator: **R. Stanley Williams**
Organization: **Regents of the University of California**

TECHNICAL REPORT No. 14

MORPHOLOGIES OF SOLID SURFACES PRODUCED FAR FROM EQUILIBRIUM

by

R.S. Williams, R. Bruinsma and J. Rudnick

Prepared for publication in

Proceedings of the Materials Research Society Symposia

University of California, Los Angeles
Department of Chemistry & Biochemistry and Solid State Sciences Center
Los Angeles, CA 90024-1569

DISCLAIMER NOTICE

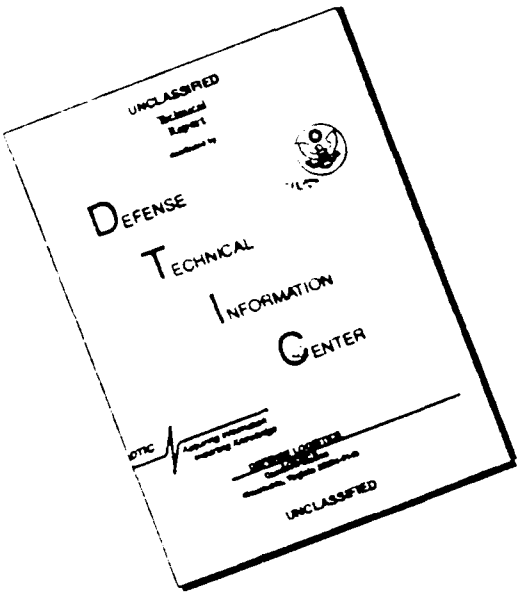

THIS DOCUMENT IS BEST QUALITY AVAILABLE. THE COPY FURNISHED TO DTIC CONTAINED A SIGNIFICANT NUMBER OF PAGES WHICH DO NOT REPRODUCE LEGIBLY.

REPORT DOCUMENTATION PAGE

Form Approved
OMB No 0704-0188

1. AGENCY USE ONLY (Leave blank)	2. REPORT DATE	3. REPORT TYPE AND DATES COVERED
	10 March 1991	Technical 6/1/91-5/31/92

4. TITLE AND SUBTITLE
MORPHOLOGIES OF SOLID SURFACES PRODUCED FAR FROM EQUILIBRIUM

5. FUNDING NUMBERS
N00014-90-J-1178

6. AUTHOR(S)
R.S. Williams, R. Bruinsma and J. Rudnick

7. PERFORMING ORGANIZATION NAME(S) AND ADDRESS(ES)
Regents of the University of California
University of California
405 Hilgard Ave.
Los Angeles, CA 90024

8. PERFORMING ORGANIZATION REPORT NUMBER
Technical Report # 14

9. SPONSORING/MONITORING AGENCY NAME(S) AND ADDRESS(ES)
Office of Naval Research
Chemistry Program
800 N. Quincy Street
Arlington, VA 22217-5000

10. SPONSORING/MONITORING AGENCY REPORT NUMBER

11. SUPPLEMENTARY NOTES
Prepared for publication in Proceedings of the Materials Research Society Symposia

12a. DISTRIBUTION AVAILABILITY STATEMENT
Approved for public release.
Distribution unlimited.

12b. DISTRIBUTION CODE

13. ABSTRACT (Maximum 200 words)

We present the first quantitative experimental study of the morphology of amorphous solid surfaces formed by non-equilibrium processes and compare the results with theories developed to explain the formation of such surfaces.

14. SUBJECT TERMS

15. NUMBER OF PAGES
19 pages

16. PRICE CODE

17. SECURITY CLASSIFICATION OF REPORT	18. SECURITY CLASSIFICATION OF THIS PAGE	19. SECURITY CLASSIFICATION OF ABSTRACT	20. LIMITATION OF ABSTRACT
Unclassified	Unclassified	Unclassified	UL

MORPHOLOGIES OF SOLID SURFACES PRODUCED FAR FROM EQUILIBRIUM

R. Stanley Williams*, Robijn Bruinsma** and Joseph Rudnick**
*Department of Chemistry and Biochemistry
University of California Los Angeles
Los Angeles, CA 90024-1569
**Department of Physics
University of California Los Angeles
Los Angeles, CA 90024-1547

ABSTRACT

We present the first quantitative experimental study of the morphology of amorphous solid surfaces formed by non-equilibrium processes and compare the results with theories developed to explain the formation of such surfaces.

1. INTRODUCTION

The preparation of surfaces and the growth of thin films are areas of great technological importance, with applications including such diverse fields as optics, chemical analyses, fabrication of microelectronic and recording devices, containment vessels for fusion reactors and manufacture of composite materials. A feature common to all these applications is that the surface preparation processes used are far from chemical equilibrium. Many of the processes involve an energetic ion beam, plasma or gas that is used to modify a surface, either by etching or depositing material. The electrical, optical and mechanical properties of the resulting systems depend strongly on the new surface morphology, which in turn depends on the kinetics of the processes that modify the surface. There have been many experimental studies of the morphology of surfaces created far from equilibrium, but so far most of these studies have been more descriptive than quantitative. With the introduction of scanning tunneling microscopy (STM) and atomic force microscopy (AFM), it is now possible to obtain a detailed three dimensional topograph of a surface $h(\mathbf{r})$, which is the height of the surface at position $\mathbf{r}$, with atomic scale resolution. One can compare the surface topographs for different processing conditions to empirically optimize the morphology of the desired surface and, as we shall demonstrate below, also understand the details of the kinetic processes that produce the observed morphology.

On the theoretical side there has been in recent years considerable progress in our understanding of the morphology of surfaces growing far from equilibrium as well as an enlarged capability for numerical simulation of film-growth under realistic conditions. On the experimental side, the STM presents us with a tool with unprecedented possibilities for quantitative characterization of surfaces over length scales ranging from 1Å up to 10^4Å. In particular, we can measure the topographical profile of the height of the surface $h(\mathbf{r})$ with a lateral resolution of 1-2Å and a vertical resolution better than 1Å for a rough surface. From $h(\mathbf{r})$, we can calculate the height-correlation function in reciprocal space, $\langle |h(\mathbf{q})|^2 \rangle$, which has become the focus for the theoretical descriptions referred to above. Thus, the STM allows us to obtain "real-space" and "momentum-space" representations of a surface on a side by side basis, whereas most electron or photon scattering techniques can only be used to obtain $\langle |h(\mathbf{q})|^2 \rangle$, because of the loss of phase information.

A) Sputtering

Sputtering is the most commonly used technique for the preparation of technologically relevant thin films.[1-3] The sputter process deposits fairly energetic atoms or ions on a growing surface. The incoming particles move along ballistic trajectories predominantly along the normal to the substrate surface. Once they reach the surface, the atoms move around by surface diffusion or by evaporation/recondensation until they reach a site where the binding energy is particularly high. At very low deposition rates, this process can preserve the crystallinity and facetting, by stepflow and island growth, as for instance described by the classical model of Burton, Cabrera and Frank.[4,5] However, for lower temperatures and economically reasonable deposition rates, the

atoms coalesce into microcrystallites and the film will be amorphous. It has been known since 1870 (!) that such films develop fascinating morphologies. The nature of the morphology depends on a variety of factors such as temperature, deposition rate and incidence angle of the beam, but the observed morphologies are commonly classified by the structure zone model (SZM) proposed by Movchan and Demchishin[7]and expanded by Thornton.[8] Our primary interest is "Zone I" with $T/T_{(melting)}$ less then 0.3 or so, where there exists a columnar fine-grained micro-structure. The boundaries between the columns are of low adatom density and they play a significant role in determining the mechanical and transport properties of the film as well as its durability and stability. Columnar structures were first observed[9] using small angle electron scattering for sputtered Pd films. Since then, there have been many reports of columnar microstructure in studies by fractography, TEM, small angle electron scattering and X-ray scattering.[10] This columnar structure has strong effects on the magnetic, optical and mechanical properties of a film.[10]

The large-scale, macroscopic morphology has been investigated in the materials-science literature since the early 1950's. Konig and Hellwig[17] first pointed out the geometrical "shadowing" effect. Protruding parts of a surface shield deeper lying sections. In particular for uncollimated incoming beams, this leads to enhancement of the surface roughness.[8] This mechanism for roughening competes with a variety of annealing mechanisms first discussed by Herring[18] At modest temperatures when the vapor pressure of the substrate is low, the dominant annealing mechanism is surface diffusion. As the vapor pressure rises, evaporation-recondensation starts to play a role. Shadowing and surface diffusion have been invoked[8]to explain the "universal" classification of thin-film microstructure: the shadowing should lead to Zone I micro-structure of low-density tapered columns with domed tops. Increased temperature increases the surface diffusion constant leading to wider, smoother columnar grains.[8] Shadowing and surface diffusion are also believed [9]to be the important factors in the evolution of rough "cone-like" surface topologies observed during sputter erosion of surfaces.[20]

There have been extensive numerical investigations of surface growth close to equilibrium.[21] Much of the earlier work was based on the solid-on-solid (SOS) model as pioneered by Gilmer[22] More recently, the growth morphology of chemical vapor deposition[23] (CVD) and molecular beam epitaxy[24] (MBE) have been investigated. Numerical studies of surfaces far from equilibrium were stimulated by observations of the microstructures of amorphous thin films. The first numerical studies of roughening due to shadowing were based on the "ballistic aggregation model" of Vold.[25] Sticky spheres were constrained to approach a substrate on straight-line ballistic trajectories. Leamy and Gilmer[26] showed that shadowing on an atomic scale produces the "tangent-rule" for the growth direction. Very large-scale simulations[27,28] of this ballistic aggregation model revealed deposits consisting of quasi-fracta[29] tree-like structure riddled with holes but obeying the tangent rule.

Real coatings, though, are smooth over distances of 100 - 1000 Å, which is the result of various annealing mechanisms. Surface diffusion can be included to some extent in computer simulations[30,31] and it indeed produces a more compact deposit. The ballistic aggregation model with surface diffusion included is thus believed to contain the basic physical mechanisms to understand the columnar structure. Because of computational limitations, at present it is difficult to perform numerical simulations on a system with more than 100 x 100 lattice constants. Thus, it is not practical to use atomic-scale simulations to study the macroscopic evolution of real columnar structures for length-scales exceeding 1000 Å and time-scales exceeding nanoseconds.

Numerical simulation of macroscopic evolution is possible if we do not attempt to describe the surface down to atomic lenghts as illustrated by the work of Srolovitz[32] and Ling and Anderson.[33] Continuum theories are thus aimed at understanding the macroscopic evolution and should be complementary to numerical studies. To model the macroscopic properties of amorphous thin-film growth, a number of continuum models have been used in the materials science literature, in particular in the context of electron-beam etching of masks for micro-electronics applications: Carter[34] reviewed a very elegant approach based on the construction of an eikonal equation for the evolution of the surface of a growing film ("Huyghens Construction") and applied it to sputter erosion. Macroscopic evolution based on shadowing was also used extensively in simulations[35] of sputter deposition onto patterned substrates. The success of these methods suggested that they could also be used for understanding the macroscopic evolution of the columnar microstructure. Continuum models have also been used for understanding the early stages of thin film evolution.[36,37]

C) Scaling Theories

Apart from the effort to model the structure of sputtered films, there has been an explosion of interest in the general features of non-equilibrium surfaces.[38] This work has centered on local growth continuum SOS models but with atomicity included through shot-noise in the incoming current. A scaling description[39-41] was proposed for this class of models in terms of the evolution of the surface roughness. Let h(r,t) be the time dependent height profile of the film. Then the height correlation function

$$C(q,t) = \langle |h(q,t)|^2 \rangle \tag{1a}$$

$$= \int \frac{d^2r}{(2\pi)^2} e^{iq\cdot r} \langle (h(0) - h(r))^2 \rangle_t / \text{Area} \tag{1b}$$

with $\langle \cdots \rangle_t$ indicating a sample average after exposure time t. This correlation function should have the general form

$$C(q,t) \propto q^{-\nu} F(t\, q^z) \tag{2}$$

would predict a power law decrease proportional to $q^{-\nu}$ in C(q,t) for $q \geq t^{-1/z}$ and $C(q,t) \sim t^{\nu/z}$ for $q \leq t^{-1/z}$. Under conditions of rotational invariance, $z = 2 - \alpha$ with $2\alpha = \nu - 2$, so there is only one free exponent (say α). This scaling law has been verified for a wide variety of local growth models.[38] Particularly influential was the KPZ model[42] where

$$\partial h/\partial t = \gamma \nabla^2 h + J + J/2\, (\nabla h)^2 + \eta(r,t) \tag{3}$$

with γ a measure of the surface annealing, J the average deposition current and $\eta(r,t)$ the shot-noise fluctuations around the average current. In "1+1" dimensions (d=1 substrate), scaling is obeyed [42] for the KPZ model with α=0.5. Many models have been investigated[43-56] and it has been found that in "2 + 1" dimensions (i.e. physical substrates) α depends on the degree of non-linearity. For very weak non-linearity (Edwards-Wilkenson Model)[57] $\alpha \rightarrow 0$ while $\alpha \rightarrow 4.0$ for strong coupling. As a function of the non-linearity there appears to be a phase-transition for discrete but not for continuum models. The connection of the KPZ model with sputtered films is that the Huyghens construction, mentioned above, can be approximated for smooth surfaces by Eq. 3 with $\gamma = \eta = 0$. Moreover, if we define an "active" surface for deposition by ballistic aggregation and fit this surface with an h(r,t), then the results appear to agree with the scaling predictions. There have, however, been few studies that investigated the experimental relevance of the scaling approach for thin film growth.[58]

II) MACROSCOPIC THEORY OF THIN-FILM GROWTH

In this section we discuss the analytical and numerical work done at UCLA aimed at investigating for the concrete case of sputtered films whether the scaling ansatz in general and the KPZ model in particular provide a viable description. The *a priori* questions were as follows:

(i) The shadow-mechanism is only local when applied to individual atoms. For a non-flat surface, shadowing is a non-local roughening mechanism. For non-local growth models (e.g. DLA) there is no reason to assume that Eq. 3 correctly gives the asymptotic (i.e. large length and time scale) properties. In particular the SOS description is invalid for DLA because the surface develops "overhangs".

(ii) Sputtered films anneal at lower temperatures by surface diffusion. This is described by a $\nabla^4 h$ term[18] rather than a $\nabla^2 h$ term, which is more appropriate for an evaporation-recondensation mechanism.[59] How does this affect the conclusions?

(iii) The surfaces of Zone I thin films look very different from those created by numerical simulation of the KPZ model. In the latter case the characteristic "domed top" and cauliflower structure of Zone I are missing. This question is related to the subsurface groove/void network. In general, SOS models cannot be expected to account for the d=3 internal structure of a film, yet the groove structure is of crucial importance for the physical properties of thin films. Of course, ballistic deposition does create an internal structure but, as we have seen, it is computationally difficult to allow annealing to proceed sufficiently to create >1000Å scale structures.

A) Column/Groove Microstructure

To answer these questions we have developed[60] a "shadow model" for the growth of the groove microstructure, based on the macroscopic description for sputtered films used in the microelectronics applications[35]. We extended these descriptions to the submicron regime by including shot-noise and surface diffusion. In this model, the local growth rate v_n is controlled by the flux $RJ(\theta)$, with $J(\theta)$ a dimensionless vector, and by surface diffusion:

$$v_n = D\, d^2\kappa/ds^2 + R \int_{\theta_-(s)}^{\theta_+(s)} J(\theta)\cdot n(s)\, d\theta + \eta(r,t) \qquad (4)$$

with D proportional to the surface diffusion constant. Next, κ is the local curvature, s the arclength (in 1+1 dimension), n(s) the local surface normal, and $\theta^{\pm}(s)$, which determine the limits of integration in Eq. 4, are the exposure angles at point s on the surface (Fig.1a). For $D=\eta=0$, this model has been very sucessful in describing the macroscopic morphology of sputtered films. (Eq. 4 is actually a generalization, due to Bales and Zangwill,[63] of our model which used the SOS approximation).

For D=0, we succeeded[60] in solving Eq. 4 analytically in the SOS approximation producing a self-similar mountain landscape. However, the columnar structure was controlled by the substrate roughness rather then by the shot-noise. Numerical simulation of Eq. 4 for $\eta=0$ by Bales and Zangwill[63] beyond the SOS approximation revealed a columnar/groove structure. The groove structure showed amazing similarity with experimental results[62] (see Fig.1b). The initial characteristic length scale of the columnar structure was again found to be set by the substrate roughness. The columnar structure appeared to coarsen with h, as noted by Messier and Yehoda, but the process could not be followed long enough because of computer limitation. The column/groove structure of Zone I is thus determined by the substrate surface roughness and not by the shot noise (as had been frequently assumed on the basis of ballistic deposition simulations). We established[62] a criterion for the initial substrate roughness to be small enough so film-quality would not be affected by column/groove microstructure. Quantitative comparisons between theory and experiment (STM studies) were found to be feasible to some extent.[62]

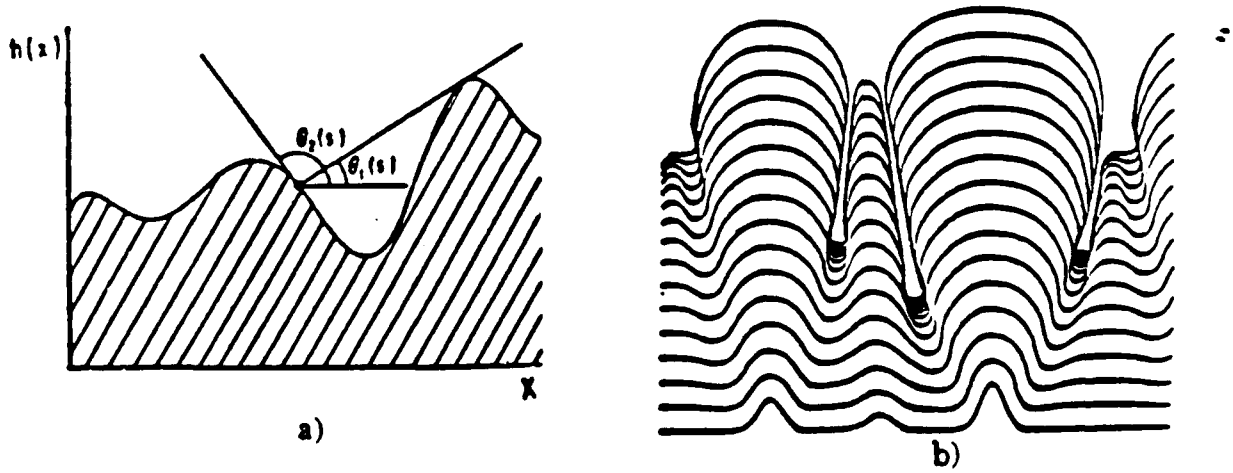

Fig. 1 a) Surface profile h(x). Incident particles can reach the surface from all directions within the cone defined by the angles $\theta_+(s)$ and $\theta_-(s)$.

b) Growth of a surface, with no shot noise, according to Eq. 4. (from ref. 62)

B) Coarsening and Scaling

The non-local algorithm for columnar growth revealed the origin of the groove structure and their connection to the initial roughness. However, the algorithm was very computer intensive and could not be used to obtain the long-time evolution of the groove structure as for instance seen in the sputter deposition of amorphous graphite films by Messier and Yehoda[12-14] To that purpose, we investigated[64] the connection between our non-local growth algorithm, and the Huyghens Construction, which is much less computer intensive. Via numerical simulation of Eq. 4 we found[64] that the Huyghens Construction actually produces mathematical singularities ("cusps") at exactly the location where the much more accurate "equation of motion" Eq. 4 produced grooves. The evolution of cusps in the Huyghens construction in the presence of noise leads to scaling for the "coarsening length" $\xi_c(h)$ (the mean distance between grooves) with exponents which agree well with experiment[12-14] In the KPZ model annealing erases the cusp

C) Surface Diffusion

We thus have found that for sputtered thin films a reasonably realistic non-local growth law (Eq. 4) can be approximated by the local Huyghens Construction. The Huyghens Construction is apparently a very powerful tool which can be used also at shorter length scales - provided the cusp singularity structure is tracked. If, with the above mentioned proviso, we can use the Huyghens Construction, does the KPZ model describe the surface structure of sputtered films correctly on length scales less than the coarsening length? Recall that on length scales less than $\xi_c(h)$, the surface of Zone I columns is (sometimes) self-similar[13]

This issue was investigated by Golubovic and Bruinsma. Surface diffusion would contribute a "$\nabla^4 h$" term and evaporation-recondensation[55] a "$\nabla^2 h$" term to the KPZ model:

$$\partial h/\partial t = D\nabla^4 h + \gamma\nabla^2 h + J + J/2\,(\nabla h)^2 + \eta(r,t). \qquad (5)$$

A renormalization group treatment demonstrated that the KPZ description for non-conservative noise[67] is valid provided γ is sufficiently positive. For pure surface diffusion, $\gamma = 0$, the surface becomes unstable towards a new fixed point because of breakdown of the SOS condition. In practice this means that KPZ can be used but only for growth problems with substantial evaporation-recondensation and for length scales less than the coarsening length $\xi_c(h)$.

Golubovic and Karunasiri[68] then investigated both analytically and numerically what will happen for pure surface diffusion, i.e. sputtering at low temperatures. They concluded that the surface will undergo a form of spinodal decomposition into a mountain landscape with cones that have a characteristic length scale that increases with time. This form of coarsening is fundamentally different from that associated with the Huyghens Construction as it is not controlled by the substrate roughness.

We thus can briefly summarize the results of the past theoretical effort as follows:

1. The column/groove microstructure is essentially a "deterministic" effect resulting from reproduction and coarsening of the initial substrate roughness through the shadowing effect.
2. If surface diffusion is the dominant annealing mechanism then the surface evolves via a spinodal decomposition mechanism leading to a coarsening mountain structure. If there is substantial annealing by evaporation/recondensation, then the scaling theories should apply.

III. EXPERIMENTAL STUDIES

This section will present the status of experimental studies. First, we will briefly review the techniques that have been used in the past to characterize deposited films and rough surfaces. Then, a substantial portion of this section will present the results and analyses of our studies of sputter etching of graphite surfaces. The discussion will demonstrate the general data collection and analysis tools that we have developed and will continue to follow in our future work, since they are substantially different from anything that has been done previously. Sputter etching and rapid film growth share the same surface annealing characteristics, so the analyses are valid for

both cases. It will also show the value of having a joint theoretical/experimental effort, since the two sides of the project have reinforced each other greatly.

A) Review of Analyses of Rough Surfaces

As mentioned previously,[9,10] the only method used in the past to obtain information about C(q) for the surfaces of sputtered films was low-angle scattering of electrons or x-rays[69-71] Historically, these experiments were very important for determining the structural properties of rough surfaces, but it is not possible to reconstruct h(r) from C(q) because the phase information is lost in the scattering process. Thus, scattering experiments must be supplemented if one is to obtain a real-space picture of the rough surface.

A great deal of experimental work involving rough surfaces has been performed with different forms of microscopy,[12-14] especially scanning electron microscopy (SEM) and transmission electron microscopy (TEM). An advantage of electron microscope techniques is that they can be used to obtain valuable information about the cross section and internal structure of a film, as long as the sectioning process does not damage the film too heavily. This is especially useful in characterizing intergranular voids and grooves. However, most researchers do not obtain a quantitative height profile of the surfaces they investigate, but rather analyze the lateral inhomogeneities of the surface by examining the variation in the gray scale of their micrographs. One of the major results from this work is the near universality of the cauliflower morphology that is observed on films of essentially anything grown under the proper conditions by a vapor deposition process.[12-14]

Rasigni et.al.[72,73] have developed a method to obtain quantitative height profiles of rough surfaces. They use a microdensitometer to digitize the gray scale of a TEM image of a carbon replica of the surface, and then assign a height scale to the digitized image based on various calibrations they can make. They have been primarily concerned with calculating various moments that characterize the surface, such as the autocovariance function (or real-space height-height correlation function), defined by

$$G(|r_2 - r_1|) = \langle h(r_2)h(r_1)\rangle - \langle h(r)^2\rangle. \qquad (6)$$

This function, which is the Fourier transform of C(q) from Eq. 1 above, is used by Rasigni et al.[72,73] primarily to characterize the degree of roughness of the surface, the length scale over which correlation of surface structure appears and to model the scattering of light from their rough surfaces. They have not related G(r) to any theories of film growth, although they could simply Fourier transform it to find C(q) and follow the prescriptions outlined above. The problems with this TEM technique are that it is very labor intensive, forming the carbon replicas can damage the surfaces on which they are made, and the resolution is no better that 100Å.

Most of the film growth studies performed with STM have involved relatively smooth surfaces produced by evaporation of films onto flat substrates.[74,75] Denley has emphasized the study of rough surfaces with STM.[76] He showed that the roughness of an evaporated Au film, defined as the average peak-to-peak height of the surface over an area imaged in a STM topograph, depended strongly on the temperature of the substrate during the deposition. He observed that the surface roughness was minimized for a substrate temperature of 300°C, which demonstrates the importance of kinetic processes even for evaporated films. He has also used STM topographs to determine the fractal dimension of rough surfaces, in an attempt to characterize different roughening processes.

Schönenberger et al.[77] have used STM to study conducting films of Fe_3O_4 deposited onto Si (100) substrates by sputtering. The surfaces of the deposited material were characterized by the now familiar domelike terminations of columnar grains of oxide with lateral dimensions in the 200-500 Å range. The mean diameter of the grains and the surface corrugation increased significantly with increasing substrate temperature, with the rms corrugation always 10% of the grain diameter. The domes were smooth and featureless. The results that were obtained depended strongly on the tips that were used, with etched Au and PtIr thermocouple wire tips producing the smallest tip artifacts in the images. The authors did not have a theoretical model to explain the morphology of their surfaces.

Poirier and White[78] have examined the effects of ion bombardment and annealing on TiO_2 (001) surfaces, and then examined the growth of Rh films on the rutile surface. They have observed that bombarded surfaces roughen, and that the rough surfaces become smoother with the initial stages of annealing. However, after annealing for 2 hours at 510°C, the surface roughens again to expose (011) and (114) facets. When Rh is evaporated onto an unfaceted surface, it forms a cauliflower pattern on the rutile. The STM topographs of these various surfaces are qualitatively similar to those collected in our laboratory from graphite surfaces sputtered etched at the higher ion doses. This is an indication of the universality of the processes that occur for etching and deposition of material from the vapor.

The recent work of Mitchell and Bonnell[79] on the analysis of sputter-deposited films and rough fracture surfaces by STM is the closest to ours in terms of the manner in which the data are represented. These researchers accumulate single STM line scans of their surfaces with 1000-2000 data points in the scan. Each scan is then Fourier transformed to yield a high quality power spectrum, and several of the power spectra are averaged to further improve the signal to noise ratio. If a substantial portion of the plot of the logarithm of the power spectrum versus the logarithm of the wavenumber is linear, then the surface displays a fractal character over the corresponding length scales and the fractal dimension is related to the slope of the line segment. At the present time, these characterizations have not been extended to the understanding of the mechanisms that give rise to the particular fractal dimensionality that is observed.

There have been several STM studies of sputtered surfaces,[80-89] but most of them have emphasized the very low ion dose limit so that they could examine the damage created by a single ion impact with the surface[80-87] or examine surface morphology after the removal of a single monolayer of material[88,89] For the case of ion bombardment of graphite with 50 keV Ar^+ ions, the surface is characterized by hillocks rather than depressions at the ion-impact sites.[85-87] These hillocks, which are roughly 10Å in radius and 1Å high, are presumed to be the result of interplanar stresses caused by the collision cascade that leads to a local volume expansion of the graphite.[87] The atomic order of the surface in the area around the hillocks is also severely distorted. Michely and Comsa[88,89]have examined the initial stages of ion etching of single crystal metal surfaces such as Pt(111) with keV energy He^+ and Ar^+ ions. With the heavier projectile, which has a sputter yield > 1, the surfaces are characterized by hexagonal vacancy islands. For He^+, which has a sputter yield << 1, the surfaces exhibit a variety of hillocks, adatom islands, and dislocations that intersect the surface. In all of these studies, the surfaces were still dominated by the structures of the underlying substrate material.

B) STM Analysis of Sputter-Etched Graphite

In contrast to the above sputtering studies, we have examined surfaces bombarded with intermediate ion doses designed to remove between 10 and 1000 atomic layers from the substrate. The surface chosen for our initial investigations was the cleaved (0001) face of highly oriented pyrolytic graphite (HOPG). This surface is inert in air and is easily imaged with the STM[83-86] Graphite also has a rigid lattice, with a melting temperature of ~3800°C. This indicates that surface diffusion should be minimal at room temperature and thus bombardment induced topography is "frozen in" and can be observed with the STM long after sputtering has occurred. Aside from experimental convenience, sputtering of graphite is intrinsically interesting to many different communities of researchers. Besides its basic theoretical interest, this work has relevance to the investigation of plasma-surface interactions at the limiters in tokamac reactors,[90] the mechanisms of diamond film growth,[91] and erosion of surfaces of composit materials in low earth orbit.[92]

Freshly cleaved graphite samples were examined with the STM before sputter etching. The STM was operated at atmospheric pressure in the constant current mode, with a tunnel current of 0.5 nA and a sample to tip bias of -100 mV. The tips used were either made from Au or PtIr wire. Low magnification topographs (2400 Å x 2400 Å image size) showed atomically flat areas over many thousands of square Ångstroms, while at higher magnifications (25 Å x 25 Å) the atomic scale features of clean graphite were easily observed.

After stable images of clean graphite were obtained, the samples were transferred to the sample treatment chamber of a KRATOS XSAM-800 surface analytical system. The graphite surfaces were sputter etched with a beam of 5 keV Ar^+ ions, rastered over a 9 mm^2 area on the sample and incident at an angle of 60° to the surface normal. The beam flux incident on the sample was determined by using an electrometer to measure the ion beam current. A small positive bias

(45 volts) was applied to the sample to suppress secondary electron emission. The experimental parameters that have been varied so far were the flux J incident on the sample, the total ion fluence $Q = Jt$ for a given exposure time t, and the substrate temperature T.

The graphite samples were re-examined with the STM after etching using identical operating parameters and, if possible, the same tunneling tip used prior to sputtering. The results shown here were reproducible from sample to sample and even with different tunneling tips. The surfaces were stable for several days, but after prolonged exposure to the air tip noise dominated the images. The images used for the data analysis were usually collected within a couple of hours of the first removal of the sample from the vacuum chamber.

The study of rough surfaces with an STM presents special problems associated with the tip and various imaging artifacts that may arise. Asymmetric tips produce artificial anisotropy in the images and blunt tips will fail to resolve closely spaced features.[93] Surfaces with very sharp protrusions will yield images of the sides of the tunneling tip instead of the surface features.[94] We have been very careful to characterize and understand these artifacts. First, we always scan a cleaved graphite surface with the tips that are used to image a rough surface to ensure that the tip is capable of producing atomic-resolution images that are free of distortion. Second, we collect dozens of images from each sample to make certain that features are reproducible and that the features scale properly as the image area is changed. Finally, we analyze the images to determine the average and maximum slopes of the features that are imaged. In all the sputtered sample work on which we have reported, the surface structures never form an angle greater than 35° with respect to the horizontal plane of the sample. We do observe structures that can be attributed to tip imaging artifacts, but images with such features are never included in our data analysis.

So far we have analyzed over 1,000 STM topographs collected from more than 15 bombarded samples. The three different incident ion fluxes reported here were $J_1 = 6.9 \times 10^{13}$, $J_2 = 3.5 \times 10^{14}$ and $J_3 = 6.9 \times 10^{14}$ ions/cm^2 sec. By varying the time of exposure to the ion beam, the total fluences obtained were $Q_1 = 10^{16}$, $Q_2 = 10^{17}$ and $Q_3 = 10^{18}$ ions/cm^2, which correspond to removing 10, 100 and 1000 monolayers of carbon, respectively, assuming a sputter yield of one atom per ion.[95,96] A matrix of STM topographs collected for the three fluxes and three fluences is shown in Fig. 2, with the lateral scale of 2400Å for all the images. In addition to the ambient temperature experiments, etching was also performed at substrate temperatures of approximately 600K and 900K for the J_2 flux and Q_2 fluence, with the corresponding topographs shown in Fig. 3. The surface roughness has been greatly exagerated in the topographs because of the expanded z-axis scale. One feature of the data presented in Fig. 2 that surprises many people is the strong dependence of the surface morphology on the ion flux. Based on the results of the theoretical work at UCLA described above, we anticipated that the flux would be important and therefore intentionally performed experiments to character the flux dependence.

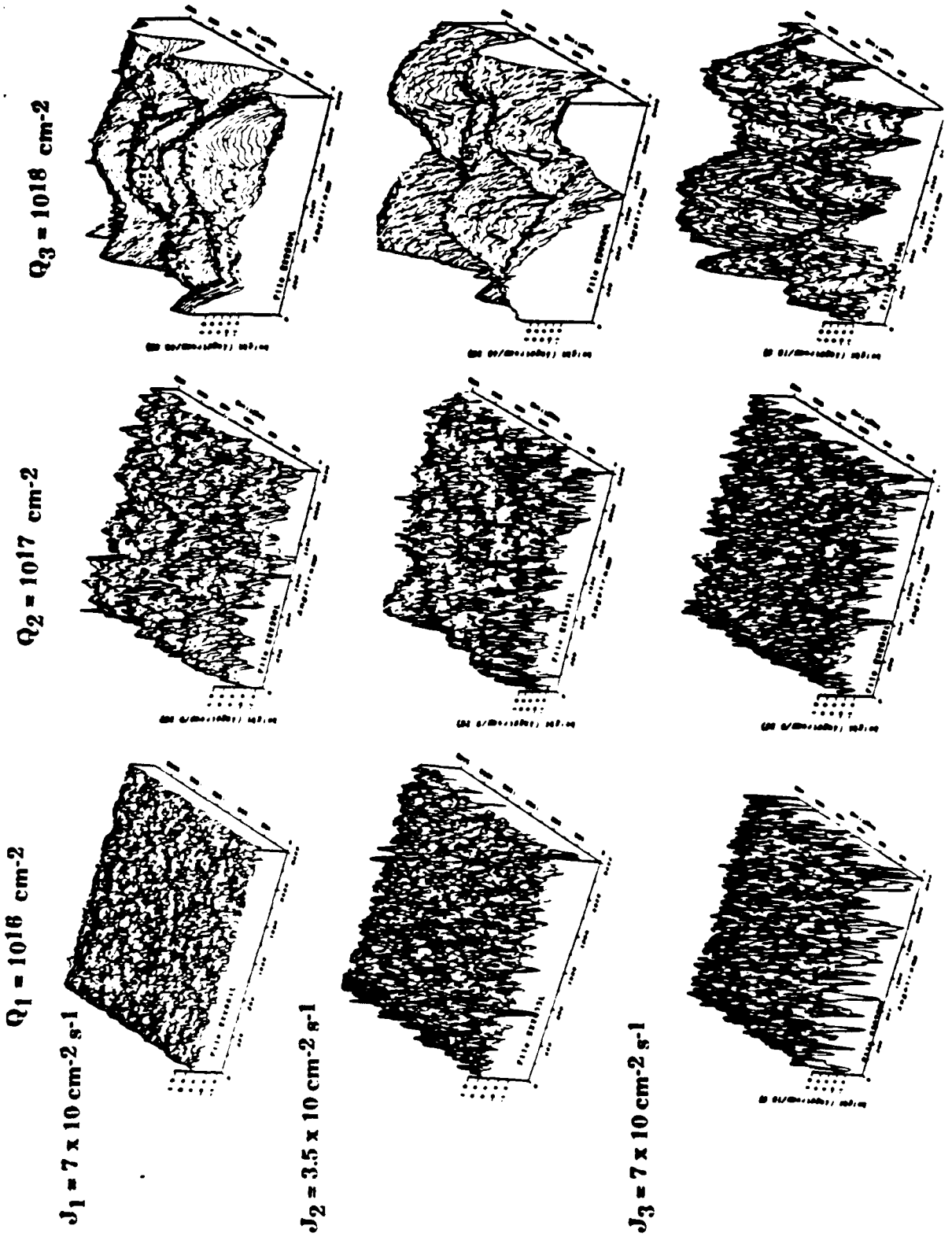

Fig. 2 Matrix of STM topographs of graphite surfaces sputtered with 5 keV Ar ions. The columns and rows of the matrix are labeled with the fluences and fluxes that caused the roughening for each surface imaged. The images all represent 2400 x 2400Å regions of the surfaces, and the scale perpendicular to the surface varies from image to image. The surface roughness is greatly exagerated so that the different surface features can be emphasized.

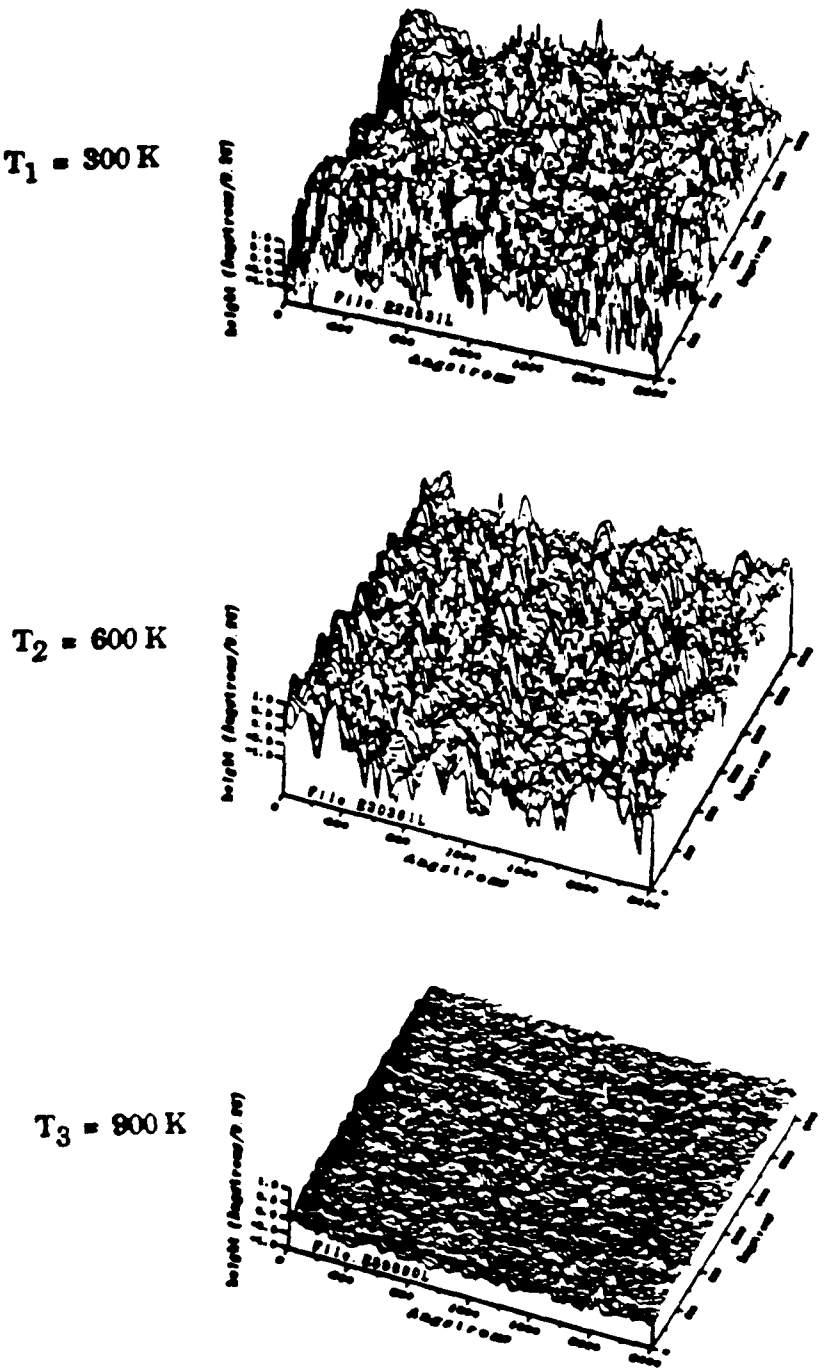

Fig. 3 STM topographs for surfaces sputtered with flux J_2 and fluence Q_2. The surfaces were held at approximately 300, 600 and 900K during the sputtering process. Elevated temperatures result in surfaces that are much smoother.

The primary new feature that we have brought to this research area is the analysis of the data, which is assisted greatly by the coupling between the theoretical and experimental groups. The calculation of the auto-covariance function G(r) with Eq. 6 provided a quantitative determination in real space of the surface roughness and the short range lateral correlation.[72,73] Selected plots of G(r) vs. r are shown in Fig. 4. For a totally random surface, G(r) resembles a delta function; G(0) is the variance of the surface height h(r) (or the square of the interface width δ)[72,73] and G(r>>0)=0. The fact that the peaks in the G(r) plots of Fig. 4 have a finite autocovariance length λ means that the surfaces have some type of correlation in their structure, which is not often visible in the STM topograph. Higher fluxes produce more disordered surfaces (smaller λ), whereas higher fluences produce more correlated surfaces (larger λ).

Selected correlation functions C(q) calculated with Eq. 1 from the height profiles of Figs. 2 and 3 are shown in Fig. 5.

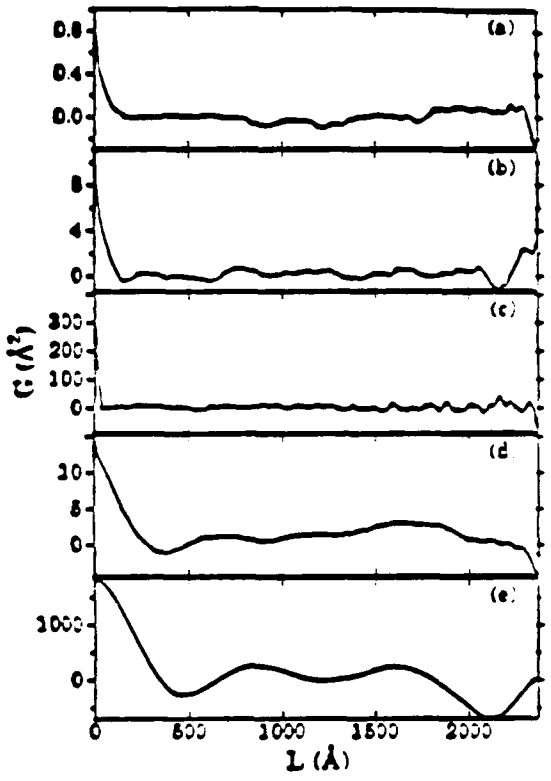

Fig. 4

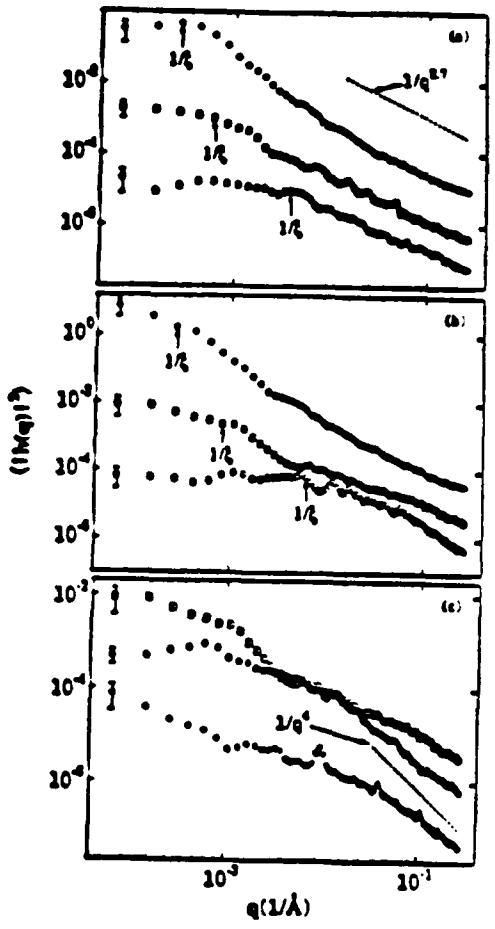

Fig. 5

Fig. 4 Plots of the autocovariance function G as a function of length for selected surfaces imaged in Fig. 2. The interface width δ is the square root of G(0), and the autocovariance length λ is indicated on each of the plots. The conditions for the plots are as follows: (a) J_1, Q_1; (b) J_2, Q_1; (c) J_3, Q_1; (d) J_1, Q_2; and (e) J_1, Q_3.

Fig. 5 Height correlation functions:

(a) $\langle |h(q)|^2 \rangle$ for the data in Fig. 2, with $Q = 10^{16}$ ions/cm^2 (○), 10^{17} ions/cm^2 (■), and 10^{18} ions/cm^2 (◇). The crossover wavevector $q_o = 1/\xi$ is indicated for each curve and a $1/q^{2.7}$ dependence is shown for comparison in the large q regime.

(b) $\langle |h(q)|^2 \rangle$ for topographs with the same parameters as in Fig. 5a, except that the flux is higher: $J = 3.5 \times 10^{14}$ ions/cm^2 sec. Note that there is a significant flux dependence, with $\langle |h(q)|^2 \rangle$ larger (the surfaces are rougher) for the higher flux.

(c) Temperature dependence of $\langle |h(q)|^2 \rangle$ from Fig. 3, with J_2, Q_2 and the temperature of the substrate T = 300K (▯), T = 600K (●) and T = 900K (♦). A $1/q^4$ dependence is shown for comparison in the large q regime. Note that $\langle |h(q)|^2 \rangle$ decreases (the surfaces are smoother) with increasing T.

The average $\langle |h(q)|^2 \rangle$ was obtained for each sample by summing the two-dimensional power spectrum, $|h(q)|^2$, over the azimuthal angle at increments of 1° for each value of q. The variance of C(q) was also calculated to provide the error bars in Fig. 5 for the correlation function of each sample. If the surface is random, C(q) will be a constant for all values of q, but if correlation is present in the surface features C(q) will have some functional dependence on q. Examining the behavior of the correlation function allowed us to determine the scaling behavior of the surfaces as a function of the wavevector q and to make comparisons to the theories of sputter erosion morphology.[97,98] Because of the absence of phase information in the height correlation function, however, it is less sensitive to uncorrelated -- but prominent -- surface features, which are much more easily visible in the real-space STM topographs. Thus, having both types of data available for exactly the same region of the surface helps greatly in understanding the structure of the surface.

The creation of correlated structures by particle radiation, which is a stochastic process that might be expected to form a totally random surface, at first seems counter-intuitive. However, the theoretical analyses of the previous section showed that the correlation arises from the various surface healing mechanisms, such as surface diffusion and evaporation-recondensation. We examined a linear version of Eq. 5 above and tested its predictions by comparing the asymptotic limits to our experimental data.[97,98] In the linear response approximation

$$\partial h(\mathbf{q},t)/\partial t = - w(\mathbf{q})\, h(\mathbf{q},t) + \eta(\mathbf{q},t) \ , \tag{7}$$

where $w(\mathbf{q})$ is the q-dependent healing rate of a surface modulation of wavevector $\mathbf{q}$ and $\eta(\mathbf{q},t)$ is the reciprocal-space shot noise term. For the case of isotropic radiation erosion, which was not strictly valid because the sample was etched by an ion beam, and including annealing by an evaporation/recondensation-like mechanism and surface diffusion, the healing rate is

$$w(\mathbf{q}) \propto J|q| + \gamma |q|^2 + D|q|^4, \tag{8}$$

with J the flux, γ the healing rate for redeposition, and D proportional to the surface diffusion constant. Equation 7 can be solved analytically to yield the correlation function :

$$C(q,t) \propto \frac{J}{w(q)} \left[1 - \exp(-2w(q)t)\right] . \tag{9}$$

By expanding the exponential in Eq. (9) one can see that for small q, C(q,t) is proportional to t and independent of q, while for large q, C(q,t) is proportional to $w(q)^{-1}$ and therefore must decrease with q. Thus, there are two distinct regions in plots of C(q,t) vs. q at any given value of t and Fig. 5 shows that this type of behavior is observed experimentally. The transition should occur at the crossover wavevector $q_0 = \xi^{-1}$, defined by $w(\xi^{-1})t = 1$, which predicts that the correlation length ξ at the knee in the C(q,t) vs. q curve is proportional to the fluence Q = Jt (assuming $\xi \lesssim (D/J)^{1/3}$). From Fig. 5a, we see that ξ increases with Q, albeit more slowly than linearly. In Fig. 5b, we show C(q,t) for the same three fluences as for Fig. 5a, but with J increased by a factor of 5. Indeed, within the uncertainties of the experimental data, ξ does not appear to have changed significantly for surfaces sputtered with the higher flux, even though these surfaces were rougher, i.e. had larger values of C(q,t), for all values of q.

We also investigated the limiting behavior of C(q,t) for large values of q. At this limit, the healing function $w(q) \propto \gamma q^2 + Dq^4$, so that C(q,t) should decrease at least as fast as q^{-2}, depending on the relative values of γ and D. The observed functional dependence for samples sputter etched at roughly 300K is $C(q,t) \propto q^{-2.7}$, so apparently two different mechanisms are involved in the healing process. Since the diffusion constant D is strongly temperature dependent, a q^{-4} tail should characterize C(q,t) for surfaces sputtered at elevated temperatures. In Fig. 5c, we show C(q,t) for graphite samples that were sputtered at temperatures T = 300, 600, and 900K. Above

600K, C(q,t) drops more sharply with q and, for large q, has a tail with an approximately q^{-4} dependence. At the lower surface temperatures, the q^{-2} healing process is apparently more important. The substrate temperatures during sputter etching are much too low for the process responsible for the q^{-2} behavior of C(q,t) to be evaporation/recondensation. However, the incident ions create a localized thermal spike when hitting the surface that can result in the formation of impact craters. Thus, the q^{-2} mechanism for healing the surface might be characterized as a "sputter/redeposition" process in which atoms move from one spot on the surface to another as flying debris from the impact of the ion.[14]

By expanding the exponential term in Eq.(9) for the limit $q \rightarrow 0$, we see that the interface width, $W = \langle |h(q \rightarrow 0)|^2 \rangle_t^{1/2}$, should be proportional to $(Jt)^{1/2} = Q^{1/2}$, a prediction which is *independent* of the healing rate function, w(q), and consistent with the stochastic nature of particle radiation. For large Q (ie. long times) and $q > 0$, the exponential term is small and can be neglected, making C(q,t) *independent of the fluence*, i.e. there should be a saturation value Q_S above which C(q,t) does not change with increasing fluence (in real space the morphology would still evolve, but the moments characterizing the surface would not). From the experimental results in Figs. 5a and 5b, we see the surprising result that W increases more like Q than $Q^{1/2}$ and that C(q,t) shows a significant dose dependence at large q. Thus, the linear response theory qualitatively accounts for the smoothening processes that lead to correlated structures on sputtered graphite surfaces, but it does not provide a quantitative description of our data because it fails to predict the Q dependence of the roughening.

We also compared the general scaling description described earlier (Eq. 2) to our experimenal data. In Fig. 5a, we see an approximate power law dependence in the correlation function at large q for the *lower* ion doses, with an associated exponent ν of order -2.5 to -2.9, resulting in $z \sim 1.6 - 1.8$ and $\nu/z \sim 1.5$. This would mean that for small q, $C(q,t) \sim t^{\nu/z}$ should increase *faster* than linearly with increasing time (or fluence), while the correlation length at crossover, $\xi \sim t^{1/z}$, should increase *more slowly* than linearly. Both predictions are valid for the experimental data collected to date. The values of α obtained from our experiments are ~ 0.2 - 0.4, which corresponds to the regime of weak nonlinearity discussed in the previous section. The results embodied in Fig. 5 thus appear to be consistent with local growth models, at least at lower fluences, which illustrates the close relationship between sputter etching and film growth.

In summary, we obtained quantitative height profiles for the initial stages of sputter etching (removal of 10-1000 monolayers) of an initially smooth surface. Ion bombarded graphite surfaces evolve a rough morphology characterized by the divergence of the correlation length, as predicted by linear response theory. By examining the q-dependence of the height correlation function, we were able to determine that two healing mechanisms, sputter/redeposition and surface diffusion, were important for forming the correlated structures on the surface. However, the experimental height-height correlation function is not quantitatively consistent with a linear response model, because it does not predict the correct fluence dependence of the surface roughening, but does have features in common with the scaling theory for sputter growth. Our work is the first to relate quantitative experimental data on the morphology of solid surfaces formed by nonequilibrium processes to the theories that have been developed to explain their formation

This work was supported in part by the Office of Naval Research.

REFERENCES

1. J. L. Vossen and W. Kern, *Thin-Film Processes* (Academic Press, New York, 1978).

2. C. R. M. Grovenor, H.T.Z. Hentzell and D.A. Smith, Acta Met. **32**, 773 (1984).

3. R. Messier, A. P Giri and R. A Roy, J. Vac. Sci. Technol. **A 2**, 500 (1984).

4. W. K. Burton, N. Cabrera and F. C. Frank, Phil. Trans. Roy. Soc. (London) **A 243**, 299 (1951).

5. W. K. Burton and N. Cabrera, Disc. Farad. Soc. **5** , 38,40 (1949).

6. I. J. Hodgkinson and P.W. Wilson, CRC Crit. Rev. Sol. State and Mat. Sci **15** 27 (1988).

7. B. A Movchan and A. V. Demchishin, Phys. Met. Metallogr. **28**, 83 (1969).

8. J. A Thornton, Ann. Rev. Mat. Sci. **7**, 239 (1977).

9. R. H. Wade and J Silcox, Appl. Phys. Lett. **8**, 7 (1966).

10. A. Dirks and H.J. Leamy, *Thin Solid Films* **47**, 219 (1977).

11. J.M. Nieuwenhuisen and H. B. Haanstra, Phillips Tech. Rev. **27**, 87 (1966).

12. R. Messier and J.E. Yehoda, J. Appl Phys. **58**, 3739 (1985).

13. J.E. Yehoda and R. Messier, Appl. Surf. Sci. **22/23**, 590 (1985).

14. R. Messier and R.C. Ross, J. Appl Phys. **53**, 6220 (1982).

15. S.C. Moss and J. F. Graczyk, Phys.Rev.Lett. **23**, 1167 (1969); M.H. Brodsky and R.S.Title, Phys.Rev.Lett. **23**, 581 (1969) and F.L. Galeener, Phys.Rev.Lett. **27**, 1716 (1971)

16. H.J. Leamy and A. G. Dirks, J. Appl Phys. **49 (6)**, 3430 (1978).

17. H. Konig and G. Helwig, Optik **6**, 111 (1950); L. Reimer, Optik **14**, 83 (1957).

18. C. Herring, J. Appl Phys. **21**, 301 (1950) and in *Structure and Properties of Solid Surfaces*, eds. R. Gomer and C.S. Smith (University of Chicago, Chicago, 1953), pp. 5-72, see discussion on pg. 64.

19. S.M. Rossnagel, in *Erosion and Growth of Solids Stimulated by Atom and Ion Beams*, G.Kiriakidis, G. Carter and J. L. Whitton, eds. (Martinus Nijhoff, Dordrect, 1986),pp. 181-199.

20. R.S. Williams, R.J. Nelson and A.R. Schlier, Appl. Phys. Lett. **36**, 827 (1980), for a review, D.D. Vvedensky, S. Clarke, K.J. Hugill, A.K. Myers-Beaghton and M.R. Nilly in *Kinetics of Ordering and Growth of Surfaces*, NATO, A S I Series, **239**, ed. M. Lagally (Plenum, New york, 1990).

21. G.H. Gilmer and K. A. Jackson, *Crystal Growth and Materials*, eds. E. Kaldis and H. J. Scheel, North Holland, Amsterdam, 1977).

22. B.J. Palmer and R. G. Gordon, *Thin Solid Films*, **158**, 313 (1988); G.S. Bales, A. C. Redfield and A. Zangwill, Phys.Rev.Lett. **62**, 776 (1989).

23. S.V. Ghaisas and A. Madhukar, J. Appl Phys. **65**, 1888 (1989), and references therein.

24. M. Rasigni, G. Rasigni, F. Varnier, C. Dussert, J. Palmari, and N. Mayani, "Statistical Analysis of Rough and Random Surfaces," in *Surface Measurement and Characterization*, J. M. Bennett, ed., Proc. SPIE 1009, pp. 68-76 (1989).

25. M.J. Vold, J. Colloid Interface Sci. **14**, 168 (1959).

26. H.J. Leamy and G.H. Gilmer, *Current Topics in Materials Science*, **6**, E. Kaldis, ed. (North-Holland, Amsterdam, 1980), pp. 309 - 344.

27. P. Meakin, J. Colloid Interface Sci. **105**, 240 (1985); D. Bensimon, B. Shraiman and S.Liang, Phys. Lett., **A102**, 238 (1984).

28. P. Meakin, CRC Critical Reviews in *Solid State and Materials Science* **13**, 143 (1987).

29. R. C. Ball and T. Whitten, Phys. Rev. **A29**, 2966 (1984).

30. K.H. Muller, J. Appl. Phys. **58**, 2573 (1985).

31. F. Family, J. Phys. **A19**, (1986) L441.

32. D. J. Srolovitz, J. Vac. Sci. Technol. **A 4**, 2925 (1986).

33. S. Ling and M.P. Anderson, J. Electr. Mat. **17**, 459 (1988).

34. G. Carter, *Erosion and Growth of Solids Stimulated by Atom and Ion Beams*, G. Kiriakidis, G. Carter and J.L. Whitton, eds. (Martinus Nijhoff, Dordrect, 1986), pp. 70-97.

35. H.P. Bader and M. A Larden, J. Vac. Sci. Technol. **B4**, 833 (1986).

36. S. Lichter and J. Chen, Phys.Rev.Lett. **56**, 1396 (1986).

37. A. Mazor, D.J. Srolovitz, P.S. Hagen and B. G. Bukiet, Phys.Rev.Lett. **60**, 424 (1988).

38. For a recent review: F. Family, Physica A, **168**, 5 61 (1990).

39. F. Family and T. Vicsek, J. Phys. **A18**, L75 (1985).

40. F. Family, *Universalities in Condensed Matter Physics*, R. Jullien, L. Peliti, R. Rammal and N. Boccara, eds., (Springer Proc. Phys.Springer Berlin, 1988).

41. T. Vicsek, *Fractal Growth Phenomena* (World Scientific, Singapore, 1989)

42. M. Kardar, G. Parisi and Y.C. Zhang, Phys.Rev.Lett. **56**, 889, (1986).

43. P. Meakin and R. Jullien, J. Phys. (Paris) **48**, 1651 (1987).

44. R. Jullien and P. Meakin, Europhys. Lett. **4**, 1385 (1987).

45. M. Plischke, Z. Racz and D. Liu, Phys. Rev. **B35**, 3485 (1987).

46. D. Liu and M. Plischke, Phys. Rev. **B38**, 4781 (1988).

47. J. Krug and H. Spohn, Phys. Rev. **A38**, 4271 (1988).

48. R. Jullien and R. Botet, J. Phys. **A18**, 2279 (1985).

49. J. G. Zabolitzky and D. Stauffer, Phys. Rev. **A34**, 1523 (1986); Phys.Rev.Lett. **57**, 1809 (1986).

50. J. Kertesz and D. E. Wolf, J. Phys., **A21**, 747 (1988).

51. D. E. Wolf and J. Kertesz, Europhys. Lett. **4**, 651 (1987).

52. J. M. Kim and J. M. Kosterlitz, Phys.Rev.Lett. **62**, 2289 (1989).

53. D. E. Wolf and J. M. Kosterlitz, Phys.Rev.Lett. **62**, 2571 (1989).

54. J. Amar and F. Family, Phys.Rev.Lett. **64** , 543 (1990).

55. T. Sun, H. Guo and M. Grant, Phys. Rev. **A40**, 6763 (1989).

56. H. Yan, D. Kessler and L. M. Sander, preprint (1989).

57. S. F. Edwards and D. R. Wilkinson, Proc. R. Soc. London, **A381**, 17 (1982).

58. For experimental tests of the scaling theory see for instance; M. A. Rubio, C. A. EdwardsA. Dougherty and J. P. Gollub, Phys.Rev.Lett. **63**, 1685 (1985).

59. W. W. Mullins, J. Appl Phys. **28**, 333 (1957).

60. R. P. U. Karunasiri, R. Bruinsma and J. Rudnick, Phys.Rev.Lett. **62**, 788 (1989).

61. R. Bruinsma, R. P. U. Karunasiri and J. Rudnick, *Kinetics of Ordering and Growth at Surfaces*, NATO A S I, Series B, **239**, M. Lagally, ed. (Plenum, 1990).

62. G. S. Bales, R. Bruinsma, E. A. Eklund, R.P.U. Karunasiri, J. Rudnick and A. Zangwill, *Science* **249**, 264 (1990).

63. G. S. Bales and A. Zangwill, Phys.Rev.Lett. **63**, 692 (1989); J. Vac. Sci. Technol.(to be published).

64. C. Tang, R. Bruinsma and S. Alexander, Phys.Rev.Lett. **64**, 772 (1990).

65. E. Medina, T. Hwa, M. Kardar and Y. Zhang, Phys. Rev. **A39**, 3053 (1989).

66. L. Golubovic and R. Bruinsma, Phys.Rev.Lett. **66** , 321 (1991).

67. For conservative (thermal) noise, Eq. 5 was investigated in ref. 55.

68. L. Golubovic and R. P. U. Karunasiri, submitted to Phys.Rev.Lett.

69. N. G. Nakhodkin, A. I. Shaldervan, A. F. Baramid, and S. P. Chenakin, Thin Solid Films **34**, 21 (1976).

70. S. C. Moss and J. F. Graczyk, Phys. Rev. Lett. **23**, 1167 (1969).

71. G. S. Cargill, III, Phys. Rev. Lett. 28, 1372 (1972).

72. G. Rasigni, M. Rasigni, F. Varnier, J. Palmari, J. P. Palmari and A. Llebaria, Surf. Sci. **162**, 985 (1985).

73. M. Rasigni, G. Rasigni, F. Varnier, C. Dussert, J. Palmari, N. Mayani and A. Llebaria, SPIE **1009** (Surface Measurement and Characterization), 68 (1988).

74. P. K. Hansma and J. Tersoff, J. Appl. Phys. **61** (2), R1 (1987).

75. H. Rohrer, in *Scanning Tunneling Microscopy and Related Methods*, R. J. Behm, N. Garcia, and H. Rohrer, eds. (Kluwer Acadedmic Publishers, Dordrecht: 1990), pp.1-26.

76. D. R. Denley, J. Vac. Sci. Technol. **A 8** (1) 603 (1990).

77. C. Schönenberger, S. F. Alvarado, and C. Ortiz, J. Appl. Phys. **66** (9) 4258 (1989).

78. Poirier and J. M. White, private communication.

79. M. W. Mitchell and Dawn A. Bonnell, J. Mats. Res. **5**, 2244 (1990).

80. I. H. Wilson, N. J. Zheung, U. Knipping and I. S. T. Tsong,Phys. Rev. B **38**, 8444 (1988).

81. I. H. Wilson, N. J. Zheung, U. Knipping and I. S. T. Tsong, J. Vac. Sci. Technol. **A 7**, 2840 (1989).

82. I. H. Wilson, N. J. Zheung, U. Knipping and I. S. T. Tsong, Appl. Phys. Lett. 53, 2039 (1988).

83. I. Kojima, N. Fukumoto, and M. Kurahashi, J. Electron Spectrosc. Relat. Phenom. **50**, c9 (1990).

84. T. C. Shen, R. T. Brockenbrough, J. S. Hubacek, J. R. Tecker, and J. W. Lyding, J. Vac. Sci. Technol. **B 9**, 1376 (1991).

85. L. Porte, M. Phaner, C. H. deVilleneuve, N. Moncoffre and J. Tousset, Nucl Instrum. Meth. Phys. Res. B **44**, 116 (1989).

86. R. Coratger, A. Claverie, F. Ajustron, and J. Beauvillain, Surf. Sci. **227**, 7 (1990).

87. L. Porte, C. H. deVilleneuve and M. Phaner, J. Vac. Sci. Technol. **B 9**, 1064 (1991).

88. Th. Michely, K. H. Besocke, and G. Comsa, Surf. Sci. Lett. **230**, L135 (1990).

89. Th. Michely and G. Comsa, J. Vac. Sci. Technol. **B 9**, 862 (1991).

90. Y. Hirooka, R. W. Conn, T. Sketchley, W. K. Leung, G. Chevalier, R. Doerner, J. Elverum, D. M. Goebel, G. Gunner, M. Khandagle, B. Labombard, R. Lehmer, P. Luong, Y. Ra, L. Schmiotz, and G. Tynan, J. Vac. Sci. Tech. **A8**, 1790 (1990).

91. J. W. Rabalais and S. Kasi, Science **239**, 623 (1988).

92. For example, Carbon Fibers, Filaments and Composites, J. L. Figueirdo, C. A. Bernardo, R. T. K. Baker and K. J. Huttinger, eds. (Kluwer Academic Publishers, Dordrecht: 1990), pp. 169-440.

93. E. J. Snyder, E. A. Eklund, and R. S. Williams, Surf. Sci. Lett. **239**, L487 (1990).

94. E. J. van Loenen, D. Dijkkamp, A. J. Hoeven, J. M. Lenssinck, and J. Dieleman, Appl. Phys. Lett. **56** (18) 1755 (1990).

95. J. F. Ziegler, J. P. Biersack, and U. Littmark, *The Stopping and Range of Ions in Solids*, (Pergammon Press, New York: 1985).

96. R. Kelly, in *Ion Bombardment Modification of Surfaces*, O. Auciello and R. Kelly, eds. (Elsevier, Amsterdam: 1984), pp. 53.

97. E. A. Eklund, R. Bruinsma, J. Rudnick and R. S. Williams, submitted to Phys. Rev. Lett.

98. E. A. Eklund, Ph.D. thesis, University of California, 1991.